❏   970

The Impact of Telemetry Received Signal Strength of IMU/GNSS Data Transmission on Autonomous Vehicle Navigation

Muhammad Khosyi'in[1], Sri Arttini Dwi Prasetyowati[2], Bhakti Yudho Suprapto[3], Zainuddin Nawawi[4]

[1,3,4]Department of Electrical Engineering, Universitas Sriwijaya, Palembang, Indonesia
[1,2]Department of Electrical Engineering, Universitas Islam Sultan Agung, Semarang, Indonesia

Article Info	ABSTRACT
	This paper presents the effect of received signal strength on IMU/GNSS sensor data transmission for autonomous vehicle navigation. A pixhawk 2.1 flight controller is used to build the navigation system. Straight lines with back-and-forth routes were tested using two types of SiK telemetry: Holybro and RFD. The results of the tests show that when the RSSI value falls close to the receiver's sensitivity value, the readings of the gyro sensor data, accelerometer, magnetometer, and GNSS compass data are disturbed. When the RSSI signal collides with noise, the radio telemetry link is lost, affecting the accuracy of speed data and the orientation of autonomous vehicles. According to Cisco's conversion table, the highest RSSI on Holybro telemetry is -48 dBm, and the lowest is -103 dBm, with a receiver sensitivity of -117 and data reading at a distance of about 427 meters. While the highest RSSI value on RFD telemetry is -17 dBm and the lowest is -113 dBm, even the lowest value is above the receiver's sensitivity limit of -121 dBm with data readings at a distance of approximately 749.4 meters. RFD outperforms Holybro in terms of RSSI and sensitivity at low data rates. When reading distance data to reference distance data using Google Earth and ArcGIS, RFD telemetry has a higher accuracy, with an average accuracy of 98.8%.

Corresponding Author:

Zainuddin Nawawi,
Department of Electrical Engineering
Universitas Sriwijaya Palembang,
Jl. Srijayanegara Palembang, 30139, Indonesia
Email: nawawi_z@unsri.ac.id

1. INTRODUCTION

The use of autonomous vehicle navigation systems is inextricably linked to the use of GPS/GNSS (Global Positioning System/Global Navigation Satellite System) sensors [1], despite GPS/flaw GNSSs of low accuracy [2], [3]. Buildings, bridges, trees, mountains, and signals reflected on flat surfaces can all interfere with GNSS reception signals. Furthermore, numerous sources of interference could potentially jam, spoof, or mitigate GPS/GNSS receivers, particularly on roads and in cities [4]. GPS/GNSS in a navigation system uses real-time geographic data from several GPS satellites to calculate longitude, latitude, speed, and direction to assist with car navigation [2].

Nonetheless, GPS and GNSS have demonstrated their ability to provide highly accurate positioning, speed, and time, which is critical for ADAS (Advanced Driver Assistance Systems) and autonomous navigation systems. With the additional correction methods, 3D locations can be as accurate as a few decimeters [4]. This further correction is typically accomplished by combining GPS/GNSS sensors with other sensors. Integrating Global Positioning System (GPS) and Inertial Navigation System (INS) for land vehicle navigation with Inertial Measurement Units (IMU) based on micro-electro-mechanical systems (MEMS-IMU) are also widely developed, but these methods also have relatively poor accuracy. Accordingly, an algorithm based on a hybrid

of the Sage-Husa filter and a robust tracking filter using a loosely coupled scheme was developed for the GPS-INS integration. This algorithm can produce superior navigation for the approximate position and speed of the vehicle [5].

Then, using Carrier-Phase Differential GPS (CPDGPS), centimeter-high AGV positioning is possible, but the GPS signal is easily attenuated or blocked. Because of this condition, this method is generally limited to open sky areas. Thus, a navigation system that combines GPS measurement and a two-dimensional laser scanner can be a solution, mainly if the GPS is not working correctly. Furthermore, most autonomous vehicle navigation systems rely on GNSS as the primary positioning sensor, even though a standalone GNSS receiver may not be capable of providing accurate positioning performance. To provide reliable navigation solutions, a navigation system method integrated with Inertial Measurement Units (IMU) and GNSS receivers is frequently used [6].

The Navigation System uses the Ground Control Station (GCS) to send sensor data and commands for autonomous vehicle navigation. The SiK radio telemetry module is used for wireless communication between the GCS and the autonomous vehicle. Previous tests show that sending data from the vehicle to the ground station with the Holybro telemetry module has problems reading sensor data because it is affected by distance and buildings [7], [8]. This is due to the Holybro's limited telemetry range of 300 meters in an open area with a standard antenna setup and a transmission power of 100 mW [9].

The current study compares the transmission of IMU/GNSS sensor data for autonomous vehicle navigation using holybro telemetry as previous research with the RFD900x telemetry module, which is claimed to have a data transmission range of up to 40 km with a transmission power of 1 W [10], [11]. This article fills a gap in previous similar research by focusing on Unmanned Aerial Vehicles (UAV) [8], [12], [13] and Unmanned Underwater Vehicles (UUV), such as autonomous boats [14], which have optimal Line-of-Sight Range due to minimal interference. The use of telemetry in ground vehicle navigation is primarily studied in terms of the performance of GPS/GNSS sensors for agricultural navigation purposes [11], [15], [16] or for Environmental Monitoring [17], with little discussion of the performance of telemetry in transmitting sensor data and its impact on navigation sensor data.

2. RESEARCH METHOD

The discussion in this research is part of the primary research on autonomous vehicle navigation systems. In this study, the navigation control system uses the pixhawk 2.1 flight controller, which is used in navigation control on Unmanned Aerial Vehicles (UAVs). SiK telemetry is commonly used to send sensor data. When implemented on a UAV, data transmission can still occur over relatively long distances because the UAV is at an altitude that allows data to be sent to GCS without being obstructed by buildings, trees, or other disturbances. It is not the same as sending sensor data from an Unmanned and Autonomous Ground Vehicle (UAGV) to the GCS. This article contributes to providing an analytical study of the impact of RSSI on telemetry for transmitting IMU/GNSS data in autonomous vehicle navigation.

2.1. Navigation System Architecture

The system architecture is based on two architectural systems: the system architecture installed on the vehicle and the system architecture installed on the ground station [7].
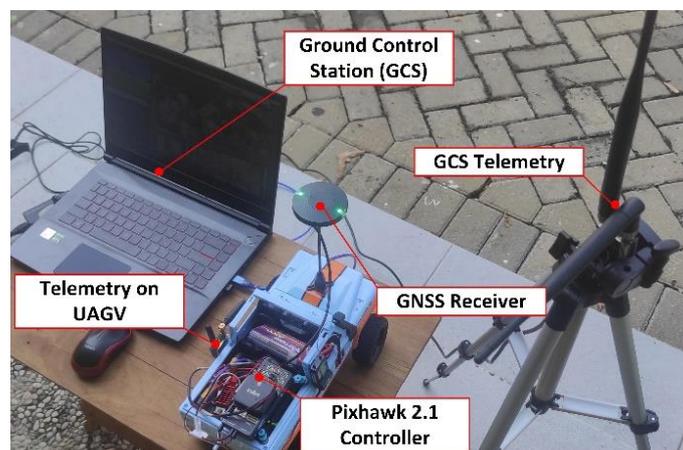
Figure 1. Navigation system architecture illustration

As shown in Figure 1, this study's sensor data collection process is carried out by installing the flight controller along with SiK telemetry on the RC car at a scale of 1:1 and another radio telemetry on the GCS

side. The RC car is placed above the vehicle and travels at a speed of 10-15 km/h to facilitate data collection. The antenna installed on the radio telemetry module is a factory default antenna with a 1 meter antenna height on the GCS side and 1.3 meter antenna height on the vehicle side. Sensor data is sent through GNSS and IMU sensor data that GCS receives via radio telemetry. This method was repeated for two types of SiK telemetry with a 915 Mhz operating frequency range. Holybro SiK Telemetry and RFD radio telemetry were used, with the specifications shown in Table 1.

2.2. System Block Diagram

This autonomous vehicle navigation system used GCS as a configuration utility, a dynamic control supplement for autonomous vehicles, or commands sent to radio control transmitters or GCS [18]. GCS is a computer device installed with the Mission Planner firmware to observe and control the autopilot controller [7].

From the block diagram of Figure 2, several devices in the navigation system installation are presented. The system was built utilizing a pixhawk 2.1 main controller with two primary sensors: IMU and GNSS Compass. The GNSS U-Blox M8N sensor was installed on the Here2 Receiver module, also equipped with IC-M20948, which functioned as a compass sensor aside from the gyro and accelerometer sensors [7], [19]. This Pixhawk 2.1 controller also had three redundant IMU systems, consisting of three accelerometers, three gyroscope sensors, three magnetometers, and three barometers, which were suitable for operating in difficult places [20]–[22].
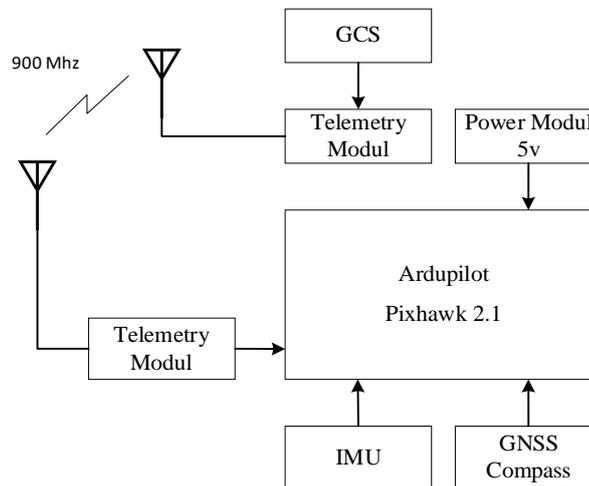
Figure 2. Configuration system block diagram

Table 1. Device specifications in system architecture

Device Name	Device Specifications	Description
Here2 GNSS Reciever	GNSS Reciever U-Blox M8N IMU/Compass: ICM20948	Installed on the controller via I2C protocol
Pixhawk 2.1 Cube Black	Pixhawk FMU Main Board: - STM32F427; flash 2MiB, RAM 256KiB - On-board 16KiB SPI FRAM - MPU9250 or ICM 20xxx integrated accel/gyro - MS5611 Baro Vibration Damped IMU board: - LSM303D integrated accel/magnetometer. - L3GD20 gyro. - MPU9250 or ICM 20xxx Gyro/Accel - MS5611 Baro	Main controller with redundant working IMU sensor, all sensors connected via SPI
Holybro SiK Telemetry	Radio Telemetry V3 with 915 Mhz Working Range, Transmit current: 100 mA at 20 dBm and -117 dBm receive sensitivity.	SiK telemetry operating at 100mW transmission power with one antenna on each modem serves to connect sensor data readings from the controller to the GCS.
RFD Telemetry	RFD 900x Long Range Telemetry Radio Modem with Frequency Band 902 MHz - 928 Mhz, transmit Power 0 to 30 dBm and Receiver Sensitivity > -121 dBm at low data rates	RFD900x Modems Operating at 1W transmission power with two dBi Monopole antennas on the Pixhawk 2.1 side and 2 Dipole antennas on the GCS

ICM-20948 is a 9-axis motion tracking device with the lowest power globally, which can be implemented for smartphones, tablets, wearable sensors, and IoT applications [23]. Input control was provided from the telemetry or companion computer, either by the radio control receiver or via MAVLink communication. The radio control receiver provided input commands for desired attitude control, vehicle power (throttle), operational mode control, and auxiliary functions. The radio control input for all navigation commands could be assigned to any radio control channel via the RCMAP_x function, while additional functions were assigned using the RCx_FUNCTION parameter [24].

2.3. Localization and Mapping

The test was carried out on a road navigation route, a two-lane road route limited by road markings with a width of about six meters in each lane, as shown in Figure 3. This route was 730 meters long and used a straight trajectory line mode with no turns. It was also the main road connected directly to the highway, with few buildings and large trees. The road markings consisted of a road island with few trees, which allowed the transmitting and receiving antennas to be completely free and unobstructed.
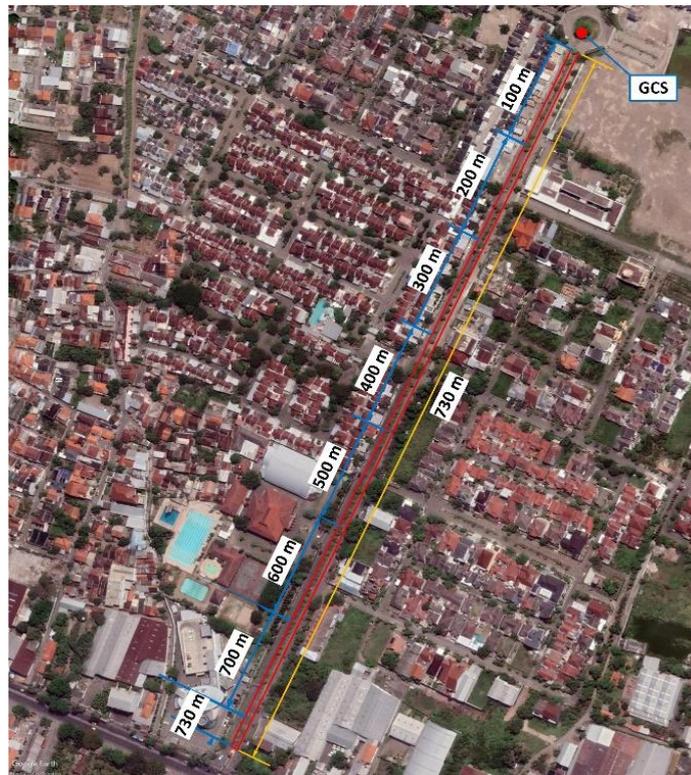
Figure 3. Map of navigation route with back-and-forth routes

2.4. Sensor Data Readout

Sensor data readings are performed on the two main sensor modules:

a. GNSS Compass Sensor Data Readout

The M8N U-Blox receiver is integrated with the Kompas Module via the IC-M20948 in the installed GNSS module. The telemetry log contains many sensor data, but only a subset is used for analysis, such as distance data, navigation traces, speed data, and vehicle orientation. Raw GPS data in the form of latitude and longitude points represented in X and Y coordinate curves with decimal degree value format is readable vehicle navigation trace data. The ArcGIS application converts the data into X and Y coordinate curves in meter format. Meanwhile, the vehicle mileage (meters) is calculated from the same GPS data, converted to meter format using the Haversine method, and compared to distance measurements obtained using the Google Earth application.

The Haversine equation was formulated with [25], [26]:

$$d = 2R\, arcsin\left(\sqrt{sin^2\left(\frac{\phi_2-\phi_1}{2}\right) + cos\phi_1 cos\phi_2 sin^2\left(\frac{\lambda_2-\lambda_1}{2}\right)}\right) \tag{1}$$

This equation is equivalent to the equation:

$$a = sin^2\left(\frac{\phi_2-\phi_1}{2}\right) + cos\phi_1 cos\phi_2 sin^2\left(\frac{\lambda_2-\lambda_1}{2}\right) \qquad (2)$$
$$d = 2R\ atan2\left(\sqrt{a}, \sqrt{1-a}\right)$$

Where atan2 is a function of MATLAB software.

To determine atan2, the spherical law of cosines (SLC) was used [27]:
$$d = R\ arccos\left(sin\phi_1 sin\phi_2 + cos\phi_1 cos\phi_2 \times cos\left(\lambda_2 - \lambda_1\right)\right) \qquad (3)$$

Where d is the distance (km), R is the radius of the earth, which is 6.371km, ϕ is latitude, and λ is longitude, where ϕ_1 refers to the start point's latitude, and ϕ_2 represents the endpoint's latitude, and λ_1 represents the start point's longitude, and λ_2 represents the endpoint's longitude, and 1 degree equals 0.0174532925 radians [28], [29].

b. IMU Sensor Data Readout
The IMU sensor is a 9-DOF (Degrees of Freedom) with a redundant operation. This type of IMU has three accelerometers, three gyroscopes measuring pitch, roll, and yaw, and three magnetometers as sensors [30]. The sensor data sampled in the shipment is IMU 1 module data, one of three sets of redundant IMU systems in the pixhawk. Accelerometer data is used to calculate vehicle acceleration (m/s^2), gyro data is used to calculate angular velocity (rad/s), and magnetometer data is used to calculate magnetic field (µT) strength.

2.5. Received Signal and Noise of SiK Radio Telemetry
This test measures the strength level of the received signal and noise from sending sensor data using the RSSI (Received Signal Strength Indicator) level and noise from each telemetry. The data used are raw RSSI data and mavlink_radio_status_t noise stored in the GCS telemetry log. RSSI (Local signal strength) indicates how strongly the GCS can receive the signal. At the same time, remRSSI (Remote Signal Strength) is an indicator of the strength and weakness of the signal received by radio on the side of the vehicle [31]. It provides a suitable communication link if the receiving remote and local signal strength is good [32]. When represented at the 0-100% level, the RSSI value is $0 - 255$ (1-byte value). It complies with the IEEE 802.11 standard, which defines the mechanism by which the circuitry measures RF energy in a wireless Network Interface Card (NIC). No vendor chooses actually to measure 256 different signal levels, so each 802.11 NIC vendor will have a particular maximum RSSI value ("RSSI_Max") [33], [34].
The RSSI value is generally presented in dBm units, and Cisco has the most detailed dBm lookup table with RSSI_Max = 100%, with a range of –10 dBm to –113 dBm. All RSSI values greater than 93% are assigned -10 dBm, and there are some places in the table where two adjacent RSSI values are given the same dBm value [33].

3.   RESULTS AND DISCUSSION
The transmission of IMU/GNSS Compass sensor data using a 915 Mhz SiK radio type holybro and RFD is a benchmark for each telemetry's characteristics in sending sensor data, precisely the effect of Receive Signal Strength on autonomous vehicle navigation data.

3.1. IMU Sensor Data Transmission Testing
The IMU is designed to predict vehicles' relative position, speed, and acceleration. It contains three sensors: an accelerator sensor that measures the acceleration of a moving object, a gyro sensor that measures rotational speed from the roll, pitch, and yaw angles, and a magnetometer sensor that measures the yaw angle (angle of deviation towards the north pole of the earth) [35].
Graphs of IMU sensor data readings transmitted via Holybro and RFD telemetry are shown in Figures 4 and 5. For approximately 340 seconds, the IMU sensor in the pixhawk installed on the vehicle runs back and forth on the navigation route (Figure 3). Accelerometer data (accelerometer), angular velocity (gyro), and magnetic field graphs are all read (magnetometer). The acceleration graph is made up of acceleration and magnetic field data for the x (forward), y (right), and z (down) directions, as determined by the sensor coordinates' direction rules. Meanwhile, the rotational speed data on the x, y, and z axes comprise the angular velocity graph. The magnetic field graph displays magnetic field data from the sensor for components in the x (forward), y (right), and z (down) directions [35]. There is no discernible difference between Figures 4 and 5. Except for the shaded period, the difference in sensor data occurs in a relatively short period and has no significant impact on the performance of each telemetry.
Figure 4 shows that IMU data transmission stopped at 142 seconds and was resumed at 315 seconds, indicating that the telemetry holybro failed to send IMU sensor data for 173 seconds. Figure 5 shows that IMU data transmission using RFD telemetry stops at 188 seconds to 229 seconds, or for 41 seconds.
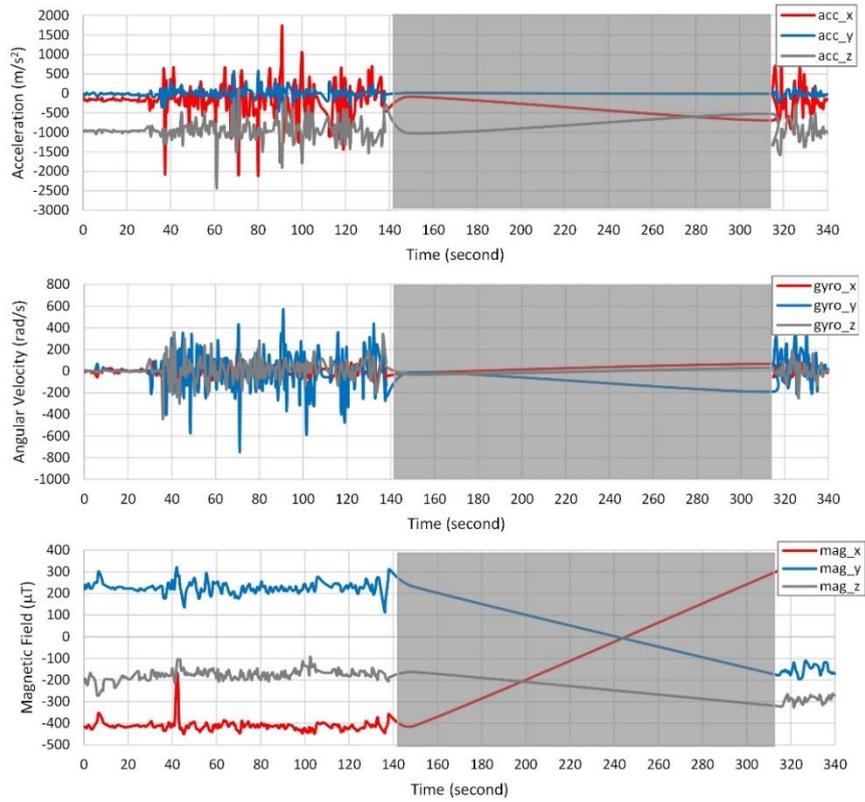
Figure 4. IMU data signal transmitted using holybro telemetry
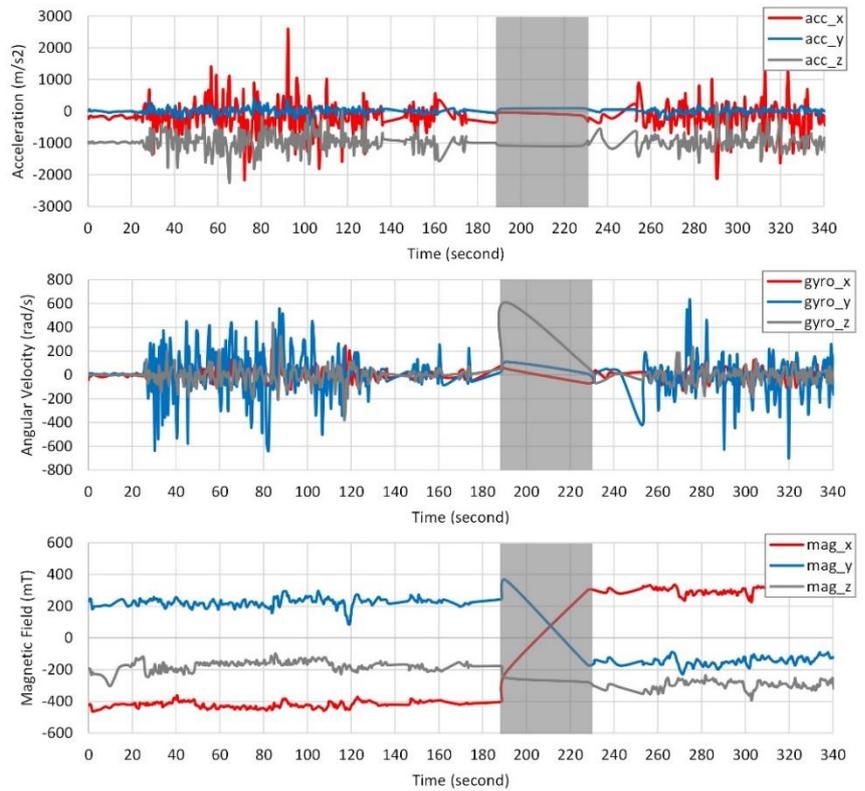
Figure 5. IMU data signal transmitted using RFD telemetry

The signal graphs depicted on the shaded time duration in Figures 4 and 5 are automatically drawn from the telemetry point when it fails to send data until it succeeds in sending data again. Telemetry failure

occurs at the greatest distance from the GCS to the vehicle or at the lowest received power value from each telemetry. In other words, with the same distance and route, Figures 4 and 5 show that RFD telemetry outperforms Holybro with the failure time duration indicator in transmitting data faster.

3.2. GPS Compass Sensor Data Transmission Testing

The next test is to read the trace trajectory to demonstrate the performance of using telemetry to send GNSS sensor data from the controller to the GCS.
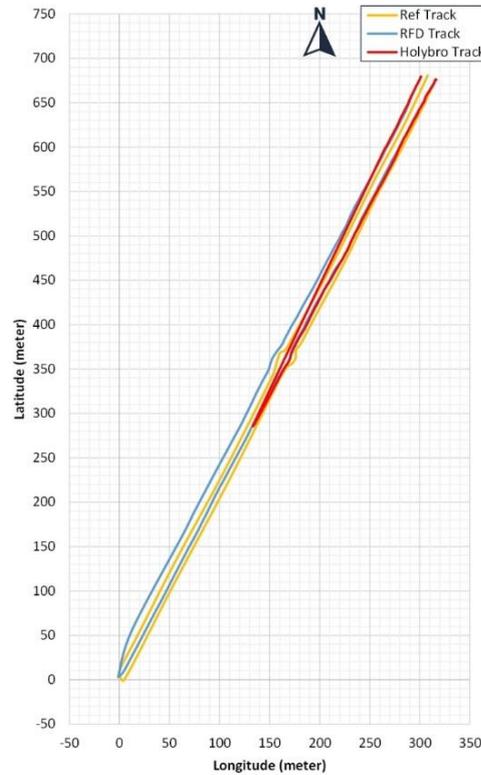
Figure 6. Navigation routes based on GNSS data in meter format

The raw GNSS sensor data is in the form of latitude and longitude, which indicate the vehicle's precise location. Latitude is defined as a line that runs north or south of the Equator and is measured from 0 degrees north or south of the Equator to 90 degrees at the poles (south and north), whereas longitude is defined as a line that runs north to south. A navigation route is generated when latitude and longitude data are represented in X and Y coordinate curves with decimal degree values. However, it is still relatively difficult to analyze the readable distance of the route range, so the data is converted into an X, Y coordinate curve in meter format using the ArcGIS application, as illustrated in Figure 6.

In Figure 6, the navigation reference route (yellow line) on the x (longitude) coordinate curve shows a value of 320 meters, and the y coordinate (latitude) is 670 meters. With a simple Pythagorean Theorem calculation, the inclined route's length equals 742.5 meters with the navigation route's direction to the southwest. These results are still relevant to the distance measured on the navigation path map, as shown in Figure 3, which is 730 meters. The difference in value is due to the rounding factor in the x and y curves.

Table 2. Measurement of vehicle mileage using the Haversine method

Telemetry	Back-and-forth mileage (m)		Farthest mileage (m)		Accuracy
	Google Earth	Haversine	Google Earth	Haversine	
Holybro	851	852.3678	427	426.1839	99.84%
RFD	1490	1495.462	745	747.7308	99.63%

Navigation routes using RFD and holybro telemetry are indicated by blue and red navigation lines, respectively. The route length successfully read from the raw GNSS data was calculated using the Haversine method according to equations 1-3. This data is then compared with measurements using Google Earth, as shown in Table 2.

According to Table 2, the GNSS data used to calculate vehicle mileage reveals that RFD telemetry has a greater range than holybro telemetry, with holybro showing the greatest distance of 426.18 meters and RFD showing the greatest distance of 747.73 meters.

When sending sensor data via telemetry, the farthest distance is assumed to be half the length of the vehicle's mileage. The haversine method produces accurate results when calculating distances measured with Google Earth. The use of Google Earth imagery is logical, and it can be used as a scientific reference for remote sensing studies [36] with fairly accurate accuracy (RMSE 0.569 ft) compared to measurements using laser theodolites [37].

When GNSS data in the form of latitude and longitude points used in measuring distances on Google Earth (Table 2) is compared with reference distances (Google Earth and ArcGIS), the distance accuracy results are obtained as shown in table 3, with an average accuracy of 58% on Holybro and 98.8% on RFD. This demonstrates the high accuracy of reading GNSS data transmitted via RFD telemetry.

Table 3. Accuracy of distance readings from GNSS data using telemetry

Ref. Distance (m)		Distance (m)		Accuracy (%)			
				to Google Earth		to Arcgis	
Google Earth	ArcGIS	RFD	Holybro	RFD	Holybro	RFD	Holybro
730	742.5	745	427	97.95	58.49	99.66	57.51

The IMU Compass sensor reading test, integrated with the GNSS sensor, shows the signal graph in Figures 7 and 8. The x curve is the duration of data transmission in seconds, and the y is velocity data in m/s units. The NED (North East Down) navigation coordinates are used, assuming that if the vx value is positive, the vehicle is moving at velocity according to the measured value on the y-axis with the heading orientation towards the north, and vice versa. If negative, it indicates the direction to the south with the velocity value shown on the graph. In contrast, if it is positive, it suggests the vehicle is moving with an orientation to the east. Negative indicates the direction to the west (the speed value always reads positive, even though the y-axis has a negative value because the negative sign is used for readings heading orientation) [35], [38].
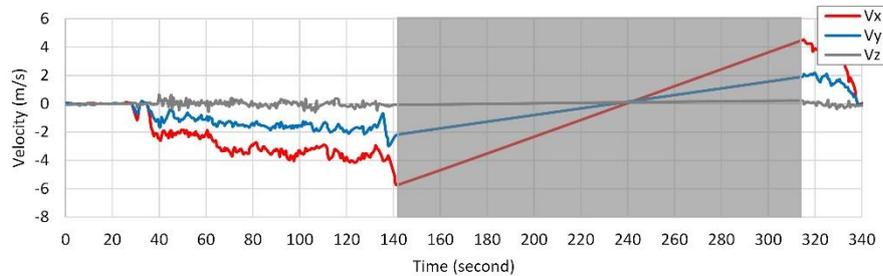
Figure 7. Transmission IMU Compass data used holybro telemetry
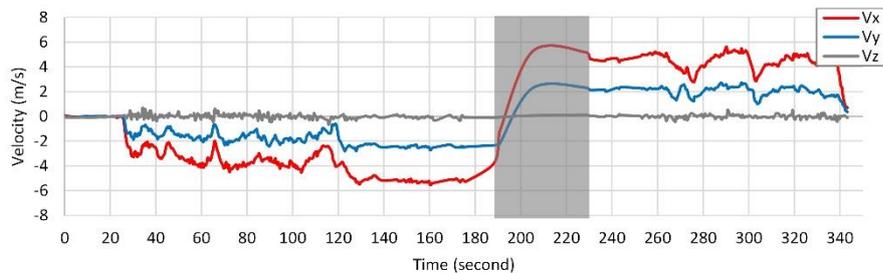
Figure 8. Transmission IMU Compass data used RFD telemetry

Figure 7 describes the vehicle movement at the velocity according to the data on the y-axis coordinate (positive speed value) in the southwest direction. The holybro telemetry cannot transmit data from the 142nd

to 315th second until it is determined that the vehicle is moving northeast (opposite to the initial direction) at the velocity value indicated by the y-axis coordinate. Figure 8 shows that the vehicle is moving southwest at the velocity value according to the data on the graph. Data reading stops at 188 seconds, and data is reread at 229 seconds with the vehicle's position moving to the northeast. The RFD telemetry cannot transmit IMU Compass sensor data for 41 seconds.

As with the previous IMU sensor readings, shaded images for a particular time duration are shown in Figures 7 and 8, illustrating that the telemetry cannot transmit GNSS compass sensor data. It can be a potential error in navigation directions and vehicle mileage. Failure to send sensor data is due to the low value of received power. According to the GNSS Compass Sensor Data Transmission test results, RFD outperforms holybro, as evidenced by more accurate mileage and navigation direction readings and a shorter duration when it fails to transmit sensor data on navigation routes with back-and-forth routes.

3.3. Telemetry Signal and Noise Measurement

The Telemetry failure in transmitting IMU/GNSS compass sensor data can be identified by monitoring the link quality. The effect of signal strength on sensor data readings is depicted in the graph. The received signal strength indicator (RSSI) and noise data were obtained from the telemetry log's MAVLink radio status reporting data.

Figures 9 and 10 show graphs of the effect of signal strength on reading distance data over 350 seconds. The x-axis represents time, the primary y-axis represents RSSI, and the secondary y-axis represents distance data. The red line represents the RSSI signal, the blue line represents the remRSSSI signal, and the green line represents the distance data. The RSSI value has been converted to dBm using the conversion table provided by Cisco [33].
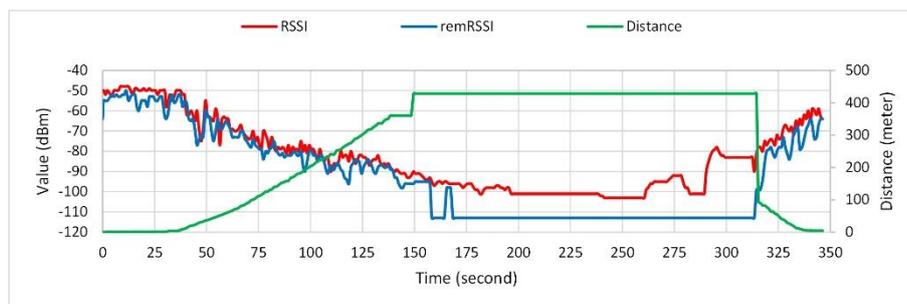
Figure 9. Graph of the effect of signal strength on reading distance data on holybro telemetry

In Figure 9, the highest rssi value identified at holybro telemetry is -48 dBm, and the lowest is -103 dBm with a receive sensitivity of -117 dBm [39]. Figure 9 shows that the measured RSSI value was -88 dBm with a reading of 360 meters at the 138th second, and the RSSI value decreased from the 150th second to the 314th second, with the lowest RSSI value of -103 dBm. During this time, the stopping distance data reading is approximately 427 meters.
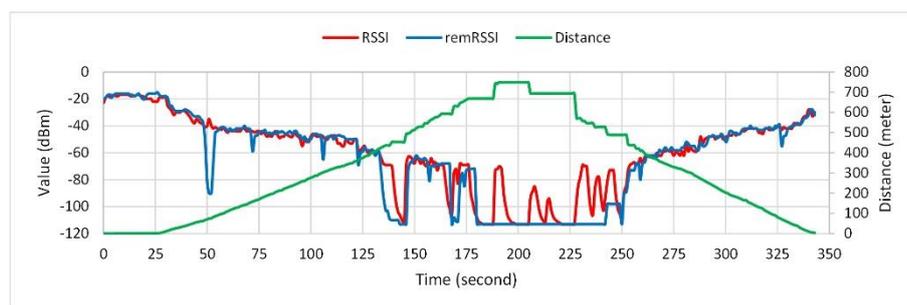
Figure 10. Graph of the effect of signal strength on reading distance data on RFD telemetry

Figure 10 shows that the RSSI value is -113 dBm beginning at the 183rd second and continues to be unstable until the 227th second, with distance data readings stopping at approximately 745 meters. According to the results of RFD telemetry measurements, the highest RSSI value is -17 dBm, and the lowest is -113 dBm. At low data rates, this lowest value is still within the receiver sensitivity limit, greater than -121dBm [40].

An analysis can be obtained by compiling data on the distance to the RSSI value, indicating that the RSSI can be used to evaluate the distance [41]. However, due to the high randomness caused by fading and

shadowing, there are limitations in building the correct relationship between the RSSI value and the distance in its implementation [42].
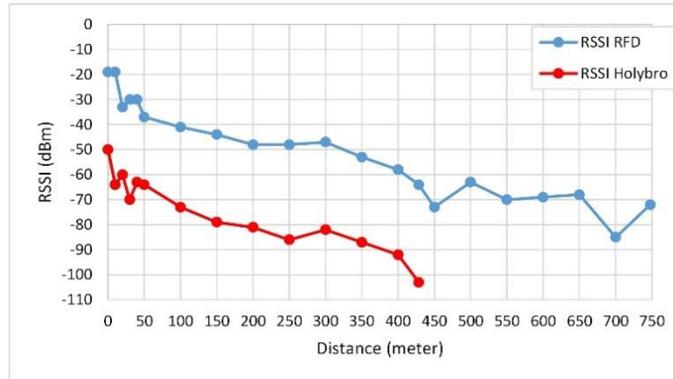
Figure 11. RSSI graph for reading distance data

Figure 11 depicts a graph of RSSI versus distance data from Holybro and RFD telemetry. The chart shows that the lowest RSSI value of the two telemetries is still above the datasheet's sensitivity limit, resulting in a higher RSSI RFD telemetry value and farther distance data reading than Holybro. Although RSSI can be used to calculate reading distance, its accuracy is poor. In other words, RSSI is an ineffective distance estimator. The dynamic fluctuations of the RSSI signal in reading distance data demonstrate this.

Figures 12 and Figure 13 depict the relationship between RSSI and noise and provide a more in-depth analysis of range problems. Noise, which is unwanted radio emission in the same frequency range as the radio frequency used to transmit data from the vehicle to the GCS, is the most common source of coverage problems.

This noise can come from a variety of sources, including electronic vehicle devices (such as motors, servos, ESC modules, and controllers), GCS devices (such as computer fans and USB port connections), and radio users operating in the same frequency range [43].

In Figures 12 and 13, noise is divided into two types: noise (the amount of noise received on the GCS) is marked with a purple line, and remnoise (the amount of noise received in the vehicle) is marked with a yellow line. The noise value on the GCS is relatively more stable compared to the remnoise, which at the same time, duration has decreased due to the influence of telemetry data transmission.
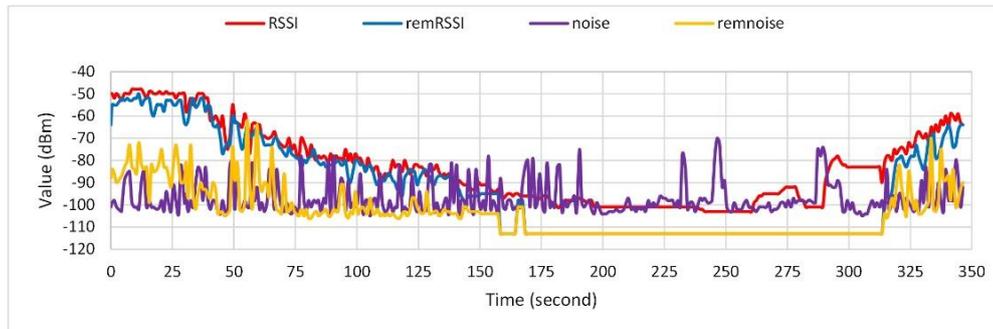
Figure 12. RSSI signal graph and noise on holybro telemetry
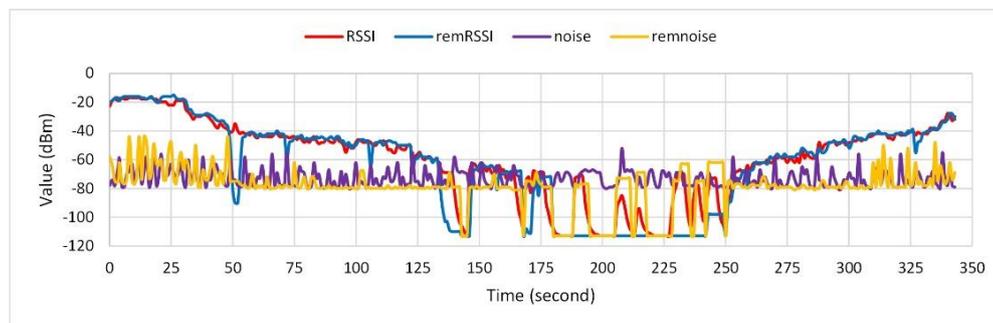
Figure 13. RSSI signal graph and noise on RFD telemetry

The graphs in figures 12 and 13 also show that when the RSSI and remRSSI signals intersect with signal noise and remnoise, the telemetry cannot transmit sensor data during this time, a condition known as lost the link [31]. This is the primary reason telemetry fails to transmit sensor data.

In the graph, RFD telemetry with proven received signal strength outperforms holybro telemetry in transmitting IMU/GNSS sensor data in autonomous vehicle navigation.

4.   CONCLUSION

The effect of telemetry received signal strength on IMU/GNSS data transmission in autonomous vehicle navigation is investigated in this study. For testing and measuring navigation sensors on a straight trajectory with back-and-forth routes, SiK telemetry 915 Mhz radios, holybro telemetry, and RFD telemetry are used. The test results show that when the received signal strength indicator (RSSI) value drops to the receiver sensitivity value, the readings of the IMU module's gyro, accelerometer, and magnetometer sensor data, as well as the GNSS Compass data, are disturbed. When the received signal strength value drops and comes into contact with signal noise, radio telemetry suffers poor link quality or even loses the link, causing navigation sensor data to be lost and affecting the accuracy of speed data or orientation headings of autonomous vehicles.

According to the Cisco conversion table from percentage to dBm, the highest RSSI on holybro telemetry is -48 dBm, and the lowest is -103 dBm, with a receive sensitivity of -117 and data readings at a distance of about 427 meters. Whereas the highest RSSI value in RFD telemetry is -17 dBm and the lowest is -113 dBm, this lowest value is still above the receiver sensitivity limit of -121 dBm with data readings at a distance of approximately 749.4 meters. When comparing the reading distance to reference distance data using Google Earth and ArcGIS, RFD telemetry has a higher accuracy in reading GNSS data, with an average accuracy of 98.8%.

REFERENCES

[1]   M. Khosyi'in, S. A. D. Prasetyowati, Z. Nawawi, and B. Y. Suprapto, "Review and Design of GPS-RFID Localization for Autonomous Vehicle Navigation," in Proceedings of the 2019 2nd International Conference on Electronics and Electrical Engineering Technology, 2019, pp. 42–46.

[2]   W. Rahiman and Z. Zainal, "An Overview of Development GPS Navigation for Autonomous Car," Proc. 2013 IEEE 8th Conf. Ind. Electron. Appl. ICIEA 2013, no. July, pp. 1112–1118, 2013.

[3]   M. Khosyi'in, E. N. Budisusila, S. A. D. Prasetyowati, B. Y. Suprapto, and Z. Nawawi, "Tests Measurement of UHF RFID for autonomous vehicle navigation," Proc. - 2020 Int. Semin. Appl. Technol. Inf. Commun. IT Challenges Sustain. Scalability, Secur. Age Digit. Disruption, iSemantic 2020, pp. 255–261, 2020.

[4]   K. von Hünerbein and W. R. Lange, "Testing Acquisition of GPS / GNSS Location and Velocity to Improve Safety in Autonomous Driving," in Proceeding-ettc2018, 2020, pp. 106–113.

[5]   H. Ahmed et al., "Adaptive Filtering on GPS-Aided MEMS-IMU for Optimal Estimation of Ground Vehicle Trajectory," Sensors, vol. 19, no. 24. 2019.

[6]   Y. Shin, C. Lee, E. Kim, and T. Walter, "Adopting Neural Networks in GNSS-IMU integration: A Preliminary study," in 2021 IEEE/AIAA 40th Digital Avionics Systems Conference (DASC), 2021, pp. 1–7.

[7]   M. Khosyi'in, E. N. Budisusila, S. A. Dwi Prasetyowati, B. Y. Suprapto, and Z. Nawawi, "Design of Autonomous Vehicle Navigation Using GNSS Based on Pixhawk 2.1," Int. Conf. Electr. Eng. Comput. Sci. Informatics, vol. 2021-Octob, pp. 175–180, 2021.

[8]   J. A. Ramirez, "Autonomous Navigation of Unmanned Aerial Vehicle in GPS," California State Polytechnic University, Pomon, 2022.

[9]   X. N. Ho and A. S. Le, Unmanned ground robot for covid-19 isolated area in vietnam, vol. 2. Springer International Publishing, 2021.

[10]   RFDesign, "RFD900ux/-SMT and RFD868ux/-SMT Radio Modem Datasheet," 7/1 Stockwell Place, Archerfield, QLD 4108, 2019.

[11]   D. S. M. Valente, A. Momin, T. Grift, and A. Hansen, "Accuracy and precision evaluation of two low-cost RTK global navigation satellite systems," Comput. Electron. Agric., vol. 168, no. August 2018, p. 105142, 2020.

[12]   J. Buele et al., "Telemetry and Video Surveillance System in a UAV for the Control and Monitoring of Long-Distance Missions," in International Conference on Computational Science and Its Applications, 2020, pp. 666–681.

[13]   S. Celidonio et al., "Platform Development for the Implementation and Testing of New Swarming Strategies," University of Maryland, 2020.

[14]   M. Thianwiboon, "Parameter Tuning of the Autonomous Boat in Fish Farming Industry with Design of Experiment," vol. 24, no. 5, pp. 217–225.

[15] R. Moeller, T. Deemyad, and A. Sebastian, "Autonomous navigation of an agricultural robot using RTK GPS and Pixhawk," in 2020 Intermountain Engineering, Technology and Computing (IETC), 2020, pp. 1–6.

[16] P. Nguyen, P. E. Badenhorst, F. Shi, G. C. Spangenberg, K. F. Smith, and H. D. Daetwyler, "Design of an Unmanned Ground Vehicle and LiDAR Pipeline," pp. 1–20, 2021.

[17] D. K. Subramaniyan, "A Mixed Aquatic and Aerial Multi-Robot System for Environmental Monitoring," The University of Toledo, 2020.

[18] ArduPilot Dev Team, "Mission Planner Overview," 2021. [Online]. Available: https://ardupilot.org/planner/docs/mission-planner-overview.html. [Accessed: 27-Jul-2021].

[19] PX4 Autopilot, "HEX/ProfiCNC Here2 GPS," 2020. [Online]. Available: https://docs.px4.io/master/en/gps_compass/gps_hex_here2.html. [Accessed: 09-Jul-2021].

[20] ArduPilot Dev Team, "The Cube Overview," 2021. [Online]. Available: https://ardupilot.org/copter/docs/common-thecube-overview.html. [Accessed: 09-Jul-2021].

[21] ProfilCNC, "Pixhawk2.1." [Online]. Available: http://www.proficnc.com/content/13-pixhawk2. [Accessed: 09-Jul-2021].

[22] C. M. D. Saraiva, "Autonomous Environmental Protection Drone," University Institute of Lisbon, 2019.

[23] T. D. K. InvenSense, "ICM-20948: World's Lowest Power 9-Axis MEMS MotionTracking Device," 2017.

[24] ArduPilot Dev Team, "Simple Overview of ArduPilot Operation," 2021. [Online]. Available: https://ardupilot.org/plane/docs/common-basic-operation.html.

[25] T. Matyja, A. Kubik, and Z. Stanik, "Possibility to Use Professional Bicycle Computers for the Scientific Evaluation of Electric Bikes: Trajectory, Distance, and Slope Data," Energies, vol. 15, no. 3, p. 758, 2022.

[26] A. Sofwan, Y. Alvin, and A. Soetrisno, "Vehicle Distance Measurement Tuning using," pp. 239–243, 2019.

[27] C. Veness, "Calculate distance, bearing and more between Latitude/Longitude points," 2022. [Online]. Available: http://www.movable-type.co.uk/scripts/latlong.html.

[28] M. Basyir, M. Nasir, and W. Mellyssa, "Determination of Nearest Emergency Service Office using Haversine Formula Based on Android Platform," Emit. Int. J. Eng. Technol., vol. 5, no. 2, pp. 270–278, 2017.

[29] S. H. Saputra and S. Nurlina, "Measure distance locating nearest public facilities using Haversine and Euclidean Methods Measure distance locating nearest public facilities using Haversine and Euclidean Methods," 2020.

[30] M. A. R. Wicaksono, F. Kurniawan, and L. Lasmadi, "Kalman Filter to Reduce Accelerometer Sensor Noise on IMU for Distance Estimation," Avitec, vol. 2, no. 2, pp. 145–159, 2020.

[31] ArduPilot Dev Team, "Telemetry (landing page)," 2021. [Online]. Available: https://ardupilot.org/rover/docs/common-3dr-radio-advanced-configuration-and-technical-information.html. [Accessed: 01-Feb-2022].

[32] R. Munusamy, J. Kumre, S. Chaturvedi, and D. Bandhu, "Design and Development of Portable UAV Ground Control and Communication Station Integrated with Antenna Tracking Mechanism," in Intelligent Infrastructure in Transportation and Management, Springer, 2022, pp. 193–212.

[33] J. Bardwell, "Converting Signal Strength Percentage to dBm Values," 1340 Treat Blvd, Suite 500 Walnut Creek, CA 94597, 2002.

[34] K. Sjöberg et al., "Measuring and using the RSSI of IEEE 802.11 p," in 17th World Congress on Intelligent Transport Systems (ITS), Busan, Korea, October 25-29, 2010, 2010.

[35] F. Kurniawan, M. R. Erdata Nasution, O. Dinaryanto, and L. Lasmadi, "Penentuan Orientasi dan Translasi Gerakan UAV menggunakan Data Fusion berbasis Kalman Filter," Avitec, vol. 3, no. 2, pp. 99–115, 2021.

[36] S. C. Benker, R. P. Langford, and T. L. Pavlis, "Positional accuracy of the Google Earth terrain model derived from stratigraphic unconformities in the Big Bend region, Texas, USA," Geocarto Int., vol. 26, no. 4, pp. 291–303, 2011.

[37] J. Wirth, E. Bonugli, and M. Freund, "Assessment of the Accuracy of Google Earth Imagery for use as a Tool in Accident Reconstruction," SAE Tech. Pap., vol. 2015-April, no. April, 2015.

[38] A. E. L. Fatimi, A. Addaim, and Z. Guennoun, "A Low-Cost IMU/GPS Position Accuracy Experimental Study Using Extended Kalman Filter Data Fusion in Real Environments," in E3S Web of Conferences, 2021, vol. 297, pp. 1–11.

[39] Holybro, "Telemetry Radio V3 915MHz," 2018. [Online]. Available: http://www.holybro.com/product/transceiver-telemetry-radio-v3-915mhz/. [Accessed: 25-Oct-2020].

[40] RFDesign Pty Ltd, "RFD900x Radio Modem Data Sheet," 7/1 Stockwell Place, Archerfield, QLD 4108, 2016.

[41] K. Benkic, M. Malajner, P. Planinsic, and Z. Cucej, "Using RSSI value for distance estimation in wireless sensor networks based on ZigBee," in 2008 15th international conference on systems, signals and image processing, 2008, pp. 303–306.

[42] V. Daiya, J. Ebenezer, S. A. V. S. Murty, and B. Raj, "Experimental analysis of RSSI for distance and position estimation," Int. Conf. Recent Trends Inf. Technol. ICRTIT 2011, pp. 1093–1098, 2011.

[43] ArduPilot Dev Team, "SiK Radio — Advanced Configuration," 2021. [Online]. Available: https://ardupilot.org/copter/docs/common-3dr-radio-advanced-configuration-and-technical-information.html. [Accessed: 19-May-2022].

BIOGRAPHY OF AUTHORS

Muhammad Khosyi'in was born on July 25th, 1979, in Jepara (Central Java, Indonesia). He graduated from Sultan Agung Islamic University (UNISSULA) Semarang with a major in electrical engineering. His post-graduate program in Electrical Engineering at Sepuluh Nopember Institute of Technology, Surabaya. And in recent years, he has taken the Electrical Engineering doctoral program at the Sriwijaya University of Palembang. He is an academic staff of Electrical Engineering at the Sultan Agung Islamic University of Semarang as a lecturer. He concerns the major control and monitoring system, electrical instrumentation, and sensor-actuator system. His last paper was "Design of Autonomous Vehicle Navigation Using GNSS Based on Pixhawk 2.1" in 2021 8th International Conference on Electrical Engineering, Computer Science and Informatics (EECSI)

Sri Arttini Dwi Prasetyowati was born on February 20th 1965 in Yogyakarta (Indonesia). She graduated from Gadjah Mada University of Yogyakarta (UGM) with a major in mathematics, and her post-graduate program was taken there. Her doctoral program is in Electrical Engineering at the Gadjah Mada University of Yogyakarta. She is an academic staff of Electrical Engineering at the Sultan Agung Islamic University of Semarang as a lecturer. She concerns in the major of signal processing. Her last paper is "Dataset Feasibility Analysis Method based on Enhanced Adaptive LMS method with Min-max Normalization and Intuitive Fuzzy Sets" in International Journal on Electrical Engineering and Informatics; Bandung, 2022.

Bhakti Yudho Suprapto was born on February 11th 1975 in Palembang (South Sumatra, Indonesia). He graduated from the Sriwijaya University of Palembang with a degree in electrical engineering. His post-graduate and doctoral program in Electrical Engineering at Indonesia University (UI) of Jakarta. He is an academic staff of Electrical Engineering at the Sriwijaya University of Palembang as a lecturer. He concerns about the major of control and intelligent system. His last paper is "Identification of Garbage in the River Based on The YOLO Algorithm" in the International Journal of Electronics and Telecommunications, 2021.

Zainuddin Nawawi was born on March 3rd 1959 in Lubuklinggau (South Sumatra, Indonesia). He is a graduate of the Sriwijaya University of Palembang with a degree in major of electrical engineering. His post-graduate and doctoral program is in Electrical Engineering at the Technology University of Malaysia (UTM). He is an academic staff of Electrical Engineering at the Sriwijaya University of Palembang as a lecturer. He concerns about the major of protection material. He is one Electrical Engineering Professor at Sriwijaya University. His last paper is "Steering control in electric power steering autonomous vehicle using type-2 fuzzy logic control and pi control" in World Electric Vehicle Journal, 2022.